Available online at www.sciencedirect.com
ScienceDirect
Scripta Materialia 59 (2008) 387–390
Scripta MATERIALIA
www.elsevier.com/locate/scriptamat

Creep resistance of cast and aged Al–0.1Zr and Al–0.1Zr–0.1Ti (at.%) alloys at 300–400 °C

Keith E. Knipling[a,b,*] and David C. Dunand[b]

[a] *Naval Research Laboratory, Code 6356, 4555 Overlook Ave, SW, Washington, DC 20375-5320, USA*
[b] *Department of Materials Science and Engineering, Northwestern University, 2220 Campus Drive, Evanston, IL 60208-3108, USA*

Received 11 September 2007; revised 18 January 2008; accepted 2 February 2008
Available online 24 April 2008

Cast and aged Al–0.1Zr and Al–0.1Zr–0.1Ti (at.%) alloys, upon compressive creep deformation at 300–400 °C, exhibit threshold stresses attributable to climb-controlled bypass of coherent Al_3Zr and $Al_3(Zr_{1-x}Ti_x)$ precipitates. Al–0.1Zr–0.1Ti exhibits a smaller threshold stress than Al–0.1Zr, which is attributed principally to a reduced lattice parameter mismatch between the $Al_3(Zr_{1-x}Ti_x)$ precipitates and the matrix. The present alloys are less creep resistant than Al–Sc and Al–Sc–Zr/Ti alloys with similar precipitate radii and volume fractions.
Published by Elsevier Ltd. on behalf of Acta Materialia Inc.

Keywords: Aluminum alloys; Zirconium; Titanium; Creep; Precipitation strengthening

The Al–Zr system exhibits particular promise for developing thermally stable precipitation-strengthened aluminum alloys [1,2]. Upon aging, supersaturated Al–Zr solid solutions nucleate Al_3Zr precipitates with a metastable cubic $L1_2$ structure (structurally and chemically analogous to the Ni_3Al γ' phase in Ni-based superalloys), which are thermally stable at high homologous temperatures.

In previous studies by the authors, the microstructures and ambient-temperature mechanical properties of conventionally solidified Al–Zr and Al–Zr–Ti alloys were studied during isothermal aging at 375, 400, 425 °C [3] and 500 °C [4] or during isochronal aging up to 600 °C [4]. Precipitation of spheroidal, nanometer-scale Al_3Zr ($L1_2$) or $Al_3(Zr_{1-x}Ti_x)$ ($L1_2$) precipitates results in a pronounced hardening response at all aging temperatures investigated. The alloys do not overage appreciably despite extended aging times (3200 h) at 425 °C ($0.75T_m$, where T_m is the absolute melting temperature of Al) [3], and only at or above 500 °C do the metastable $L1_2$ trialuminide precipitates transform to their equilibrium $D0_{23}$ structures [4]. The addition of Ti was shown to have no effect on the coarsening of the precipitates or on the onset of overaging.

Figure 1 displays the precipitated microstructure of an Al–0.1Zr–0.1Ti alloy after aging at 375 °C for 1600 h [3], and is representative of the alloys studied here. The Al_3Zr ($L1_2$) or $Al_3(Zr_{1-x}Ti_x)$ ($L1_2$) precipitates are non-uniformly distributed, reflecting the dendritic microsegregation of Zr and Ti solute atoms during solidification. The precipitate-free interdendritic channels have a deleterious effect on the ambient-temperature mechanical properties, and strengthening occurs on multiple length scales: (i) on the nanometer-scale scale by an Orowan strengthening mechanism; and (ii) on the micrometer-scale related to the volume fraction of the precipitate-rich dendrites [4]. This article investigates the mechanical properties of similar alloys, during creep experiments performed at 300, 350 or 400 °C.

The creep behavior of precipitation- or dispersion-strengthened materials generally follows a power-law equation of the form [5]:

$$\dot{\varepsilon} = A_{ap}\ \sigma^{n_{ap}}\ \exp\left(-\frac{Q}{R_g T}\right), \tag{1}$$

where $\dot{\varepsilon}$ is the minimum, secondary strain rate, A_{ap} is a constant, σ is the applied stress, n_{ap} is the apparent stress exponent, Q_{ap} is the apparent activation energy, R_g is the universal gas constant, and T is the absolute temperature. When the apparent stress exponent significantly exceeds that of the matrix, an athermal threshold stress, σ_{th}, is assumed, below which creep is negligible. This leads to a modified power-law equation [6,7]:

* Corresponding author. Address: Naval Research Laboratory, Code 6356, 4555 Overlook Ave, SW, Washington, DC 20375-5320, USA. Tel.: +1 202 767 2947; fax: +1 202 767 2623; e-mail: knipling@anvil.nrl.navy.mil

1359-6462/$ - see front matter Published by Elsevier Ltd. on behalf of Acta Materialia Inc.
doi:10.1016/j.scriptamat.2008.02.059

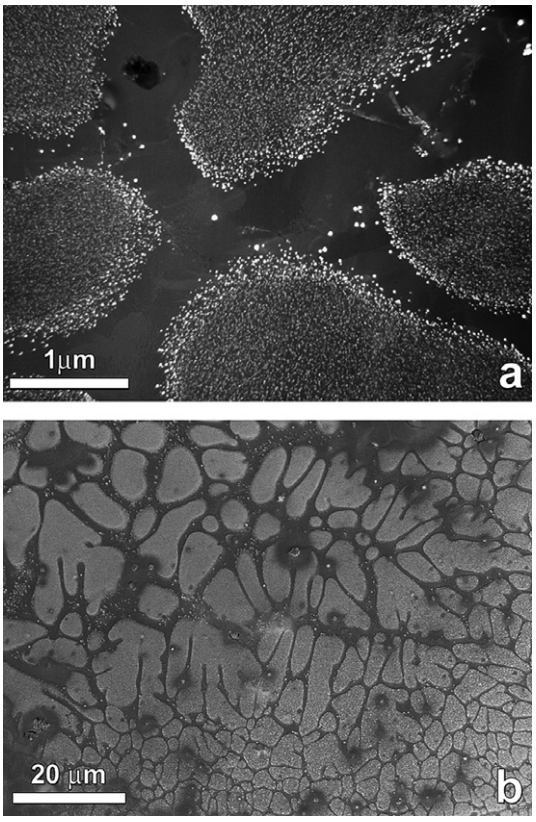

Figure 1. Transmission electron microscopy (TEM) and scanning electron microscopy (SEM) micrographs of Al–0.1Zr–0.1Ti aged at 375 °C for 1600 h [3]: (a) centered dark-field TEM images showing the dendritic distribution of nanometer-scale $Al_3(Zr_{1-x}Ti_x)$ ($L1_2$) precipitates; (b) SEM secondary electron image illustrating the inhomogeneous nature of the dendritic distribution.

$$\dot{\varepsilon} = A\ (\sigma - \sigma_{th})^n\ \exp\left(-\frac{Q}{R_g T}\right), \tag{2}$$

where A is a constant, n is the matrix stress exponent, and Q is the matrix creep activation energy, which is usually equal to the activation enthalpy for self-diffusion. For alloys with coherent unshearable precipitates and large grains, the threshold stress, σ_{th}, arises from the increase in length of the dislocation during the climb bypass [8]. An upper bound value for the threshold stress σ_{th} is the Orowan stress, σ_{or}, above which dislocations bypass dispersoids by bowing within their glide plane.

Small (~7 g) buttons with nominal composition Al–0.1Zr and Al–0.1Zr–0.1Ti and exact composition Al–0.079Zr and Al–0.081Zr–0.092 Ti (all compositions are in at.% in the remainder of this article unless otherwise noted) were prepared by non-consumable electrode arc melting, as described previously [3]. Creep specimens in the shape of parallelepipeds (approximately 4 × 4 × 8 mm) were electrode-discharge-machined (EDM) with their axes perpendicular to the surface of the ingot that had been in contact with the water-cooled copper crucible during arc melting. The height of the creep specimen spans nearly all of the button ingot height. The alloys were aged isothermally at 400 °C for 100 h prior to creep, which produces a peak-aged hardness of ~420 MPa in similar alloys investigated previously [3].

Constant-load compression creep tests, with compressive stresses in the range of 4–30 MPa, were performed in air at 300–400 °C. A superalloy creep cage translated tensile loads in the pull-rods to compressive stresses on the specimen. Frictional effects on the end-loaded specimens were minimized using alumina platens coated with boron nitride. Specimen temperature was measured in the three-zone furnace with a temperature stability of ±1 °C after a 1 h soak at the test temperature. Specimen strain was calculated from extensometric displacements of cage platens measured using a linear variable differential transducer (LVDT) with a resolution of 2.5 μm. Once steady-state deformation was achieved, the load was increased, resulting in 3–5 data points suitable for determining a stress exponent from one specimen. Total specimen strain never exceeded 10%.

During high-temperature loading, a primary creep regime, where the strain rate decreases continuously with time, always precedes steady-state creep. The strain associated with primary creep, even near the threshold stress, can be large (~2–3%), and may represent unimpeded dislocation glide through the precipitate-free interdendritic channels. The minimum strain rate from the steady-state regime is plotted as a function of applied stress in Figure 2 for tests performed at 300, 350 or 400 °C. Despite the non-uniform precipitate distribution and the associated precipitate-free interdendritic channels (Figure 1), the Al–Zr and Al–Zr–Ti alloys show remarkably high creep resistance at 300–400 °C in the low-stress regime where the apparent stress exponent, n, of both alloys is much than for pure Al ($n = 4.4$). This is indicative of the existence of a threshold stress whose values, as determined from linear fits of $\dot{\varepsilon}^{1/n}$ vs. σ [9] using $n = 4.4$ [10] for dislocation creep of Al, are indicated in Figure 2.

As discussed previously [3,4], Ti additions to Al–Zr alloys have very little effect on the kinetics of growth or coarsening of $Al_3(Zr_{1-x}Ti_x)$ ($L1_2$) precipitates as compared to Al_3Zr ($L1_2$). Because of their indistinguish-

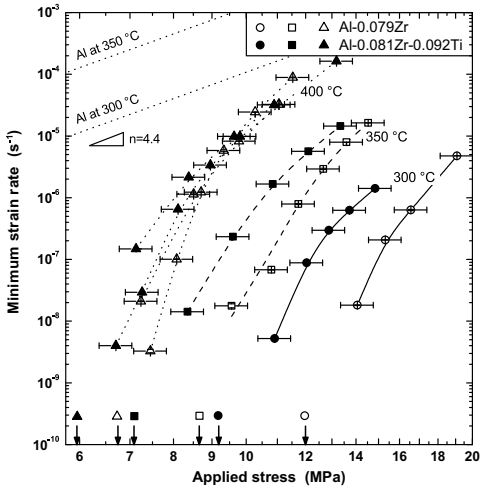

Figure 2. Double logarithmic plot of minimum creep rate at 300, 350 or 400 °C vs. applied stress, for Al–0.079Zr and Al–0.081Zr–0.092Ti alloys aged for 100 h at 400 °C. Each curve represents data from a single specimen; two specimens each of Al–0.079Zr and Al–0.081Zr–0.092Ti alloys were tested at 400 °C. The arrows indicate calculated values of σ_{th}. Data for pure Al calculated from Ref. [10].

able precipitate radii, it was expected that the Al–Zr and Al–Zr–Ti alloys would behave similarly during creep. Figure 2 indicates, however, that at a given temperature, Al–0.081Zr–0.092Ti consistently has a smaller σ_{th} than Al–0.079Zr. This is despite the higher concentration of solutes in the ternary alloy, and the higher expected volume fraction of precipitates, which results in slightly larger peak hardness at ambient temperature, observed upon isochronal aging [4] or isothermal aging above 400 °C [3]. This discrepancy between ambient and high-temperature strength may be attributable to: (i) a reduction in grain size in the ternary Al–Zr–Ti alloy; or (ii) a reduction in the lattice parameter mismatch between the $Al_3(Zr_{1-x}Ti_x)$ precipitates and the α-Al matrix, as discussed in the following.

The as-cast macrostructures of similar alloys are discussed in detail in Ref. [3]. The solidification macrostructure is typical of conventionally cast alloys, with coarse columnar grains, originating at the bottom surface of the ingot (which was in contact with the chilled copper crucible of the arc melter), growing upward toward a zone of equiaxed grains near the center of the ingot. A binary Al–Zr alloy similar to the one studied here is comprised entirely of columnar grains that are 0.2–1.0 mm wide and ~5 mm long [3]. The effect of an additional 0.1 at.% Ti results in equiaxed grains in the upper half of the ingot that are 0.5–1.0 mm in diameter. The relative size of the columnar and equiaxed zones is thus strongly dependent on the solute content of the alloy and, more precisely, on the extent of properitectic Al_3M (M=Zr or Zr, Ti) precipitation, since these primary phases are potent grain refiners in aluminum [11,12]. The refined grain structure in the ternary alloy is therefore more susceptible to grain boundary sliding, although this deformation-mechanism seems unlikely given the existence of a threshold stress. Aluminum dendrites, in the absence of heterogeneous nucleation sites, grow in crystallographically preferred ⟨100⟩ directions [13], explaining the columnar macrostructure observed for the binary alloy. Since the equiaxed microstructure of the ternary alloy is no longer textured along ⟨100⟩, differences in crystallographic texture may also explain the poorer creep performance.

A more likely explanation for the discrepancy in creep behavior is based on the prediction that σ_{th} increases significantly with the precipitate lattice parameter mismatch with α-Al, δ, due to elastic interactions from the coherent precipitates [14,15]. The lattice parameters of the present Al_3Zr ($L1_2$) or $Al_3(Zr_{1-x}Ti_x)$ ($L1_2$) precipitates were not measured directly, but may be estimated from Figure 3 using the reported values for Al_3Zr ($L1_2$) and Al_3Ti ($L1_2$), and the lattice parameters of $Al_3(Zr_{1-x}Ti_x)$ ($L1_2$) measured by Malek et al. [20]. Use of Figure 3 requires knowledge of the $Al_3(Zr_{1-x}Ti_x)$ precipitate compositions, which have been measured directly by three-dimensional atom-probe tomography for similar Al–0.1Zr–0.1Ti alloys [21]. After isothermal aging at 375 or 425 °C, the precipitates are $Al_3(Zr_{0.91}Ti_{0.09})$ or $Al_3(Zr_{0.83}Ti_{0.17})$, respectively, with corresponding ambient-temperature mismatches of $\delta = +0.43\%$ or $+0.22\%$, respectively (as determined from Figure 3). The $Al_3(Zr_{1-x}Ti_x)$ ($L1_2$) precipitates thus have a much smaller mismatch than that of Al_3Zr ($L1_2$), $\delta = 0.75\%$.

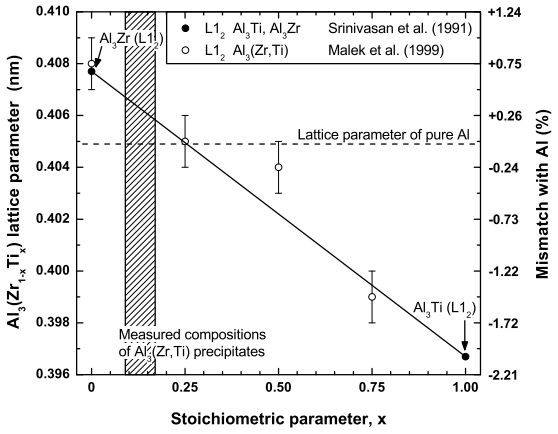

Figure 3. Dependence of the lattice parameter (at ambient-temperature) of the metastable $Al_3(Zr_{1-x}Ti_x)$ ($L1_2$) phase on the stoichiometric parameter x. Measured lattice parameters of $Al_3(Zr_{1-x}Ti_x)$ are from Malek et al. [20]. The lattice parameters of the metastable $L1_2$ Al_3Zr (0.4077 nm) and Al_3Ti (0.3967 nm) trialuminides are from Srinivasan et al. [25]. The compositions of $Al_3(Zr_{1-x}Ti_x)$ precipitates measured by three-dimensional atom-probe tomography [21], and the corresponding mismatch, are also indicated.

These mismatches are reduced further at the elevated temperatures relevant for creep, due to differences in the coefficient of thermal expansion (CTE) for the Al_3M precipitates and the α-Al solid solution. Harada and Dunand [22] measured δ as a function of temperature for Al_3Sc-based trialuminides, and observed an absolute change of -0.39% for Al_3Sc ($L1_2$) (from $\delta = 1.34\%$ at ambient-temperature to $\delta = 0.95\%$ at 400 °C). Assuming that the thermal expansion of the present Al_3Zr ($L1_2$) or $Al_3(Zr_{1-x}Ti_x)$ ($L1_2$) precipitates is similar to that of Al_3Sc ($L1_2$), δ for Al_3Zr ($L1_2$) at 400 °C should be half of its ambient-temperature value, and δ of $Al_3(Zr_{1-x}Ti_x)$ ($L1_2$) should be near-zero, or possibly negative, at 400 °C. The associated reduced elastic interactions for the $Al_3(Zr_{1-x}Ti_x)$ ($L1_2$) precipitates at elevated temperatures may explain the smaller observed creep threshold stress for Al–0.081Zr–0.092Ti as compared to Al–0.079Zr.

We now compare our results to previous creep studies on cast Al–Sc alloys. At 300 °C (see Figure 4), the Al–Sc-

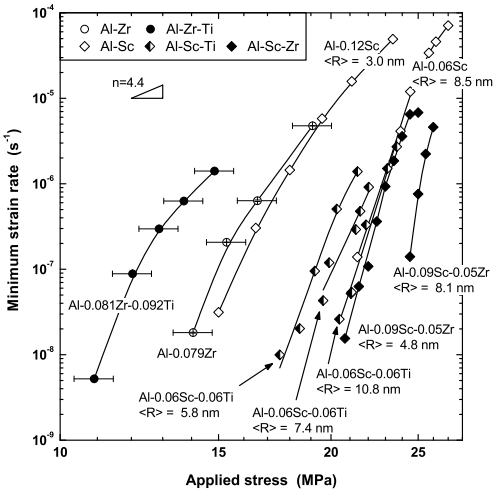

Figure 4. Minimum creep rate at 300 °C vs. applied stress, comparing data in Figure 2 to Al–Sc [16,17], Al–Sc–Zr [18] and Al–Sc–Ti alloys [19]. Mean precipitate radius, ⟨R⟩, is indicated for the Al–Sc alloys.

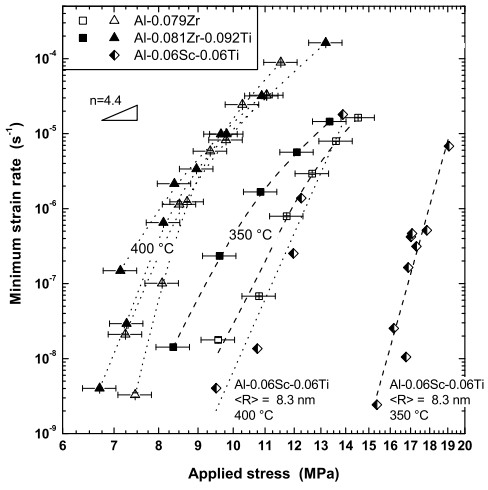

Figure 5. Minimum creep rate at 350 or 400 °C vs. applied stress, comparing data in Figure 2 to that of Al–Sc–Ti alloys [23].

based alloys outperform the present Al–Zr-based alloys, probably because of their non-uniform distribution of precipitates (Figure 1). The observed Vickers microhardness in these segregated alloys is much less than that predicted by the Orowan mechanism (based on measured precipitate radius), indicating that the non-uniform precipitate distributions are deleterious to the ambient-temperature strength [4]. This might also explain the poorer creep performance of the Al–Zr and Al–Zr–Ti alloys, as compared with the homogeneous Al–Sc alloys.

Since σ_{th} is very sensitive to δ, elastic interactions may also account for the improved threshold stress for the Sc-containing alloys. At 300 °C, the lattice parameter mismatch with α-Al of Al_3Sc ($L1_2$) is $\delta = +1.08\%$ [22], whereas that of Al_3Zr ($L1_2$) is $\delta = +0.49\%$ (assuming a similar CTE as Al_3Sc, as discussed above).

Figure 5 compares the current results to those of van Dalen et al. [23] on Al–0.06Sc–0.06Ti alloys crept at 350 and 400 °C. Here again the Zr-containing alloys exhibit smaller threshold stresses, for the same reasons discussed above (non-uniform precipitate distributions and smaller mismatch, δ). Al–0.06Sc–0.06Ti at 400 °C is comparable to Al–0.079Zr at 350 °C, despite the greater coarsening resistance of Al_3Zr ($L1_2$) as compared to Al_3Sc ($L1_2$) [3,24].

The maximum temperature investigated by creep was 400 °C because, beyond this temperature, a precipitous drop in hardness was observed during isothermal aging of similar alloys [3]. Improved results might be obtained by isochronal aging since, unlike isothermal aging, the precipitates are nucleated at the lowest possible aging temperature resulting in a larger volume fraction of precipitate-rich dendrites [4]. Moreover, isochronally aging specimens to 475 °C ($0.80T_m$) permits creep experiments at this temperature, where the alloys are still strong and the Al_3Zr ($L1_2$) precipitates are intrinsically stable. The present alloys were also not aged to the optimum precipitate size for creep. Figure 4 indicates that Al–0.079Zr has comparable creep performance to Al–0.12Sc ($\langle R\rangle = 3.0$ nm) [17]. Al–0.06Sc, despite having a smaller volume fraction of precipitates, exhibits a much-improved threshold stress, attributable to the larger precipitate radii ($\langle R\rangle = 8.1$ nm). It is assumed that $\langle R\rangle \leq 10$ nm in the present alloys, comparable to what was measured previously during extended (1600 h) isothermal aging at 425 °C [3]. This corresponds approximately to the ambient-temperature peak-aged strength, which is typically not optimum for creep.

In summary, Al–0.079Zr and Al–0.081Zr–0.092Ti (at.%) alloys were aged at 400 °C for 100 h and tested under creep conditions at 300, 350 or 400 °C. They exhibit creep threshold stresses, ~6–12 MPa, indicative of a climb-controlled bypass mechanism. For a given temperature, the ternary Al–Zr–Ti alloy exhibits a smaller threshold stress than the binary Al–Zr alloy. This disparity is assigned to a reduction in the lattice parameter mismatch of the $Al_3(Zr_{1-x}Ti_x)$ precipitates with the α-Al solid solution. Threshold stresses are also less than for Al–Sc, Al–Sc–Zr and Al–Sc–Ti alloys with similar radii and volume fractions of precipitates, because of the non-uniform distribution of precipitates in Al–Zr and Al–Zr–Ti alloys and also the smaller lattice parameter mismatch of Al_3Zr ($L1_2$) as compared to Al_3Sc ($L1_2$).

This research is supported by the US Department of Energy, Basic Sciences Division, under contracts DE-FG02-02ER45997 and DE-FG02-98ER45721.

[1] K.E. Knipling, D.C. Dunand, D.N. Seidman, Z. Metallkd 97 (2006) 246.
[2] K.E. Knipling, D.C. Dunand, D.N. Seidman, Metall. Mater. Trans. A 38 (2007) 2552.
[3] K.E. Knipling, D.C. Dunand, D.N. Seidman, Acta Mater. 56 (2008) 114.
[4] K.E. Knipling, D.C. Dunand, D.N. Seidman, Acta Mater. 56 (2008) 1182.
[5] A.K. Mukherjee, J.E. Bird, J.E. Dorn, Trans. ASM 62 (1969) 155.
[6] J.H. Gittus, Proc. Roy. Soc. Lond. A 342 (1975) 279.
[7] J.C. Gibeling, W.D. Nix, Mater. Sci. Eng. 45 (1980) 123.
[8] J. Rosler, E. Arzt, Acta Metall. 36 (1988) 1043.
[9] R. Lagneborg, B. Bergman, Metal Sci. 10 (1976) 20.
[10] H.J. Frost, M.F. Ashby, Deformation-Mechanism Maps: The Plasticity and Creep of Metals and Ceramics, Pergamon Press, New York, 1982.
[11] T. Ohashi, R. Ichikawa, Z. Metallkd 64 (1973) 517.
[12] D.G. McCartney, Inter. Mater. Rev. 34 (1989) 247.
[13] M.C. Flemings, Solidification Processing, McGraw-Hill, New York, 1974.
[14] E.A. Marquis, D.C. Dunand, Scripta Mater. 47 (2002) 503.
[15] Y. Xiang, D.J. Srolovitz, Philos. Mag. 86 (2006) 3937.
[16] D.N. Seidman, E.A. Marquis, D.C. Dunand, Acta Mater. 50 (2002) 4021.
[17] E.A. Marquis, D.N. Seidman, D.C. Dunand, Acta Mater. 51 (2003) 285.
[18] C.B. Fuller, D.N. Seidman, D.C. Dunand, Acta Mater. 51 (2003) 4803.
[19] M.E. van Dalen, D.C. Dunand, D.N. Seidman, Acta Mater. 53 (2005) 4225.
[20] P. Malek, P. Bartuska, J. Plestil, Kovove Mater. 37 (1999) 386.
[21] K.E. Knipling, D.C. Dunand, D.N. Seidman, Microsc. Microanal. 13 (2007) 503.
[22] Y. Harada, D.C. Dunand, Scripta Mater. 48 (2003) 219.
[23] M.E. van Dalen, D.N. Seidman, D.C. Dunand, Acta Mater, in press, doi: 10.1016/j.actmat.2008.05.002.
[24] E.A. Marquis, D.N. Seidman, Acta Mater. 49 (2001) 1909.
[25] S. Srinivasan, P.B. Desch, R.B. Schwarz, Scripta Metall. Mater. 25 (1991) 2513.